Non-LoS Error Mitigation Using a Sensor Fusion Approach for Indoor UWB Localization

Dae-Woong Kim[*], Joon-Yong Lee[°]

ABSTRACT

A localization technique that integrates the ultra-wideband (UWB) radio and image sensor is proposed. This positioning scheme implements an estimation algorithm utilizing the generalized maximum-likelihood (GML) or maximum-likelihood (ML) method. The test results obtained using 70 indoor measurements show improvements in performance in the presence of LoS blockage(s) between the target and the UWB beacon, compared with the use of only one of the sensors.

Key Words : ultra-wideband, image processing, sensor-fusion, localization, non-LoS error

Ⅰ. Introduction

Ultra-wideband (UWB) radio has been considered one of the most viable solutions for indoor localization. However, in non-line-of-sight (non-LoS) environments, the ranging accuracy is significantly reduced [1,2], and various methods for non-LoS identification have been suggested for performance improvement [3,6]. Studies have also been presented on the integration of UWB and other sensors, most of which are about combination of UWB with inertial sensors [7,10]. This study introduces a positioning method through integration of the UWB radio and a single image sensor. In this work, the image sensor is used for two purposes: to provide a position estimate of the target and to determine the existence of a LoS blockage between the target and each beacon. Depending on the existence of the distribution of the non-LoS ranging error, different kinds of location algorithms are introduced. The parameters used in the statistical models and algorithms are determined experimentally, and the algorithms are tested on a set of propagation measurements.

Ⅱ. Measurement system

In order to test the algorithm proposed in this study, propagation experiments were carried out in the lobby of the law school library and Hyoam chapel at Handong University. For the purpose of radiolocation, three UWB receivers were used as beacons and one transmitter as a target. The P440 radios used as transceivers manufactured by Humatics, Inc. have one omni-directional dipole antenna attached. Each radio was arranged in known locations and fixed on a 60 cm-high foam pad to reduce reflections at close distances. Samples were taken in the time domain with a sampling period of 61 ps, and the sampled waveforms were averaged

over 512 sweeps to increase the signal-to-noise ratio. The canonical single-path waveform, namely $s(t)$, can be approximated by [11],

$$s(t) = A\exp(-at^2)\sin(wt), \tag{1}$$

where $a = 5.55 \times 10^{18}$, $w = 26.15 \times 10^9$, and A is a constant. The 10 dB bandwidth of $s(t)$ is approximately 1.22 GHz (3.51-4.73 GHz) and its spectral density is shown in Fig. 1.

One C920R camera manufactured by Logitech, Inc. with 1920×1028 resolution was used as an image sensor. The camera was installed approximately 5 m above the ground and approximately $80°$ downwards. By changing the locations of the target and other objects, we controlled the number of blocked beacons between 0 and 3; 16 measurements were taken without obstacles and 18 measurements were taken in each case of one to three blocked beacons. To distinguish the target from the other objects during image processing, it was placed on a blue-colored pad.
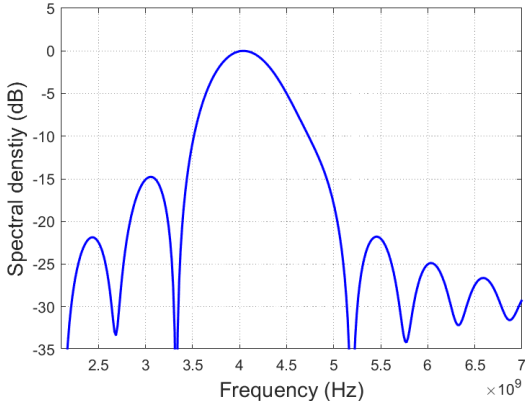

Fig. 1. Spectral density of the template waveform.

Ⅲ. UWB distance measurements

The UWB ranging algorithm used in this study is based on the method proposed in [1]. Using the CLEAN algorithm, the multipath components are decomposed and the leading edge of the received signal is detected. Let vectors $\underline{z}$ and $\underline{p}_j$ indicate the true two-dimensional positions of the target and the jth beacon, respectively. If r_j denotes the range estimate between them, the ranging error ϵ_j is given by

$$\epsilon_j = r_j - \parallel \underline{z} - \underline{p}_j \parallel . \tag{2}$$

Here, let us define a parameters N_j to indicate the existence of a LoS blockage at the jth beacon: $N_j = 1$ when the jth beacon is blocked, and $N_j = 0$, otherwise. Subsequently, ϵ_j can be expressed as

$$\epsilon_j = \begin{cases} \zeta_j, & \text{if } N_j = 0, \\ \zeta_j + \chi_j, & \text{if } N_j = 1, \end{cases} \tag{3}$$

where ζ_j is the time delay estimation error due to the pulse mismatch and χ_j denotes the bias error due to the LoS blockage. More specifically, bias error χ_j is caused by two factors: the time delay estimation error due to missed direct path and the excess propagation delay of the signal [5]. Fig. 2 shows the estimated range compared to the true distance. We can clearly see the bias errors in non-LoS case.

Random variables ζ_js are assumed to be independent and identically distributed (iid) with ζ, where $\zeta \sim N(0, \sigma_\zeta^2)$. The value of σ_ζ^2 was chosen to be 2.872×10^{-4}.
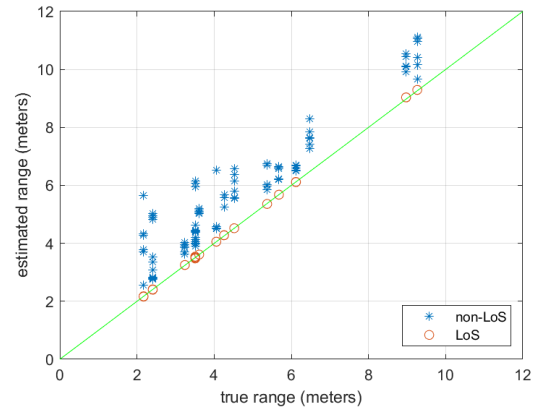

Fig. 2. Estimated range and true range.

Ⅳ. Non-LoS identification

Based on the shape or color of the object detected in the image, it is assumed that it is possible to determine whether it is a target or not. We also assume that all objects detected in the image are tall enough to block the LoS between the beacon and the target, provided it is blocked in two dimensions. Fig. 3 is a flow chart of the image processing process. Background subtraction was performed by computing the absolute difference between the current image and the background image. The binarization of the image was done first by converting the RGB image to a grayscale image using a function in the openCV library, namely cvtColor, and subsequently applying a threshold γ_g with a value of 40. An object was defined as a group of connected components with an area of more than 5,000 pixels obtained using the connectedComponents function. Taking into account the height and the angle of the camera lens with the vertical axis, the two-dimensional position of the kth object, namely $\underline{u}_k$, was defined as the location of the pixel corresponding to the mid-point of the width and 15 % of the height. Without loss of generality, the 1st detected object is assumed to be the target that we want to locate. Then, the image positioning error of the target, namely ν, is given by

$$\nu = \| \underline{u}_1 - \underline{z} \|, \qquad (4)$$

and we assume that it is an exponential random variable with a parameter λ:

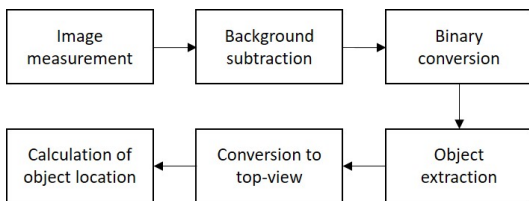$$f_\nu(\nu) = \lambda e^{-\lambda\nu}, \nu > 0, \qquad (5)$$

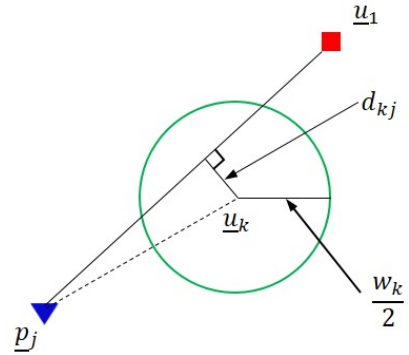Fig. 3. Flow chart of image processing for object detection.

Fig. 4. Non-LoS identification at the jth beacon.

where $\lambda = 4.368$.

The top-view transformation method employed in this work is based on the direct linear transform algorithm[12], and we used functions getPerspectiveTransform and warpPerspective.

For convenience, the two-dimensional shape of the object is assumed to be a circle with a radius of $w_k/2$ (see Fig. 4), where w_k is width of the kth object detected in the image. Let's define d_{kj} as the distance from the terminal point of $\underline{u}_k$ to the straight line connecting the terminal points of vectors $\underline{u}_1$ and $\underline{p}_j$. Then, it is determined that the jth beacon is blocked by the kth object provided that

$$\| \underline{u}_k - \underline{p}_j \| < \| \underline{u}_1 - \underline{p}_j \|, \qquad (6)$$

and

$$d_{kj} < \frac{w_k}{2}. \qquad (7)$$

Ⅴ. Position estimation

5.1 Generalized maximum likelihood estimation

In this study, different estimation techniques are applied depending on the presence of a statistical model of bias error χ_j due to LoS blockage. We apply the generalized maximum likelihood (GML) estimation method when a statistical model of χ_j does not exist. The GML estimate of the target

location can be represented by

$$
\hat{\underline{z}}_{\mathrm{GML}} =
$$
$$
\underset{\underline{z}}{\arg\max} \left[\left[\prod_{i \in \Omega} \max_{\chi_i \geq 0} f_{r_i | \underline{z} N_i \chi_i}(r_i | \underline{z}, 1, \chi_i) \right] \cdot \left[\prod_{j \in \Omega} f_{r_j | \underline{z} N_j}(r_j | \underline{z}, 0) \right] f_{\underline{u}_1 | \underline{z}}(\underline{u}_1 | \underline{z}) \right], \tag{8}
$$

where $\Omega = \{ j | N_j = 1, 1 \leq j \leq 3 \}$ is a collection of indexes of the blocked beacons. In this equation, the likelihood function is expressed as the product of the conditional densities of all measurements because they are conditionally independent. Notice that the likelihood function is maximized over χ_js with $i \in \Omega$ as their distributions are not available. Each conditional density appearing in (8) can be represented by the density of corresponding measurement error, and therefore (8) reduces to

$$
\hat{\underline{z}}_{\mathrm{GML}}
$$
$$
= \underset{\underline{z}}{\arg\max} \left[\left[\prod_{i \in \Omega} \max_{\chi_i \geq 0} f_\zeta (r_i - \parallel \underline{z} - \underline{p}_i \parallel - \chi_i) \right] \cdot \left[\prod_{j \in \Omega} f_\zeta (r_j - \parallel \underline{z} - \underline{p}_j \parallel) \right] f_\nu (\parallel \underline{z} - \underline{u}_1 \parallel) \right], \tag{9}
$$

where

$$
\max_{\chi_i \geq 0} f_\zeta (r_i - \parallel \underline{z} - \underline{p}_i \parallel - \chi_i)
$$
$$
= \begin{cases} f_\zeta(0), & r_i \geq \parallel \underline{z} - \underline{p}_i \parallel, \\ f_\zeta (r_i - \parallel \underline{z} - \underline{p}_i \parallel), & r_i < \parallel \underline{z} - \underline{p}_i \parallel. \end{cases} \tag{10}
$$

Furthermore, using the log-likelihood function, $\hat{\underline{z}}_{\mathrm{GML}}$ is calculated by

$$
\hat{\underline{z}}_{\mathrm{GML}} =
$$
$$
\underset{\underline{z}}{\arg\min} \left[\sum_{i \in \Omega} \frac{1}{2\sigma_\zeta^2} (r_i - \parallel \underline{z} - \underline{p}_i \parallel)^2 u(\parallel \underline{z} - \underline{p}_i \parallel - r_i) \right.
$$
$$
\left. + \sum_{j \in \Omega} \frac{1}{2\sigma_\zeta^2} (r_j - \parallel \underline{z} - \underline{p}_j \parallel)^2 + \lambda \parallel \underline{z} - \underline{u}_1 \parallel \right], \tag{11}
$$

where function $u(\,\cdot\,)$ denotes the unit step function.

5.2 Maximum likelihood estimation

If a statistical model of bias error χ_j is given, maximum likelihood (ML) estimation can be applied. In this section, we assume that χ_js are iid with lognormal random variable χ which satisfies [13]

$$
\ln \chi \sim N(\mu_\chi, \sigma_\chi), \tag{12}
$$

where $\mu_\chi = -0.0478$ and $\sigma_\chi = 0.551$. The ML estimate of $\underline{z}$ is given by

$$
\hat{\underline{z}}_{\mathrm{ML}} = \underset{\underline{z}}{\arg\max} \left[\left[\prod_{i \in \Omega} f_\epsilon (r_i - \parallel \underline{z} - \underline{p}_i \parallel) \right] \cdot \left[\prod_{j \in \Omega} f_\zeta (r_j - \parallel \underline{z} - \underline{p}_j \parallel) \right] f_\nu (\parallel \underline{z} - \underline{u}_1 \parallel) \right], \tag{13}
$$

where random variable ϵ is identically distributed with ϵ_js. When the jth beacon is blocked, the density of the ranging error ϵ_j is expressed as a convolution of densities of ζ_j and χ_j, as $\epsilon_j = \zeta_j + \chi_j$, and therefore, $f_\epsilon(\varepsilon)$ is given by

$$
f_\epsilon(\varepsilon) = f_\chi(\varepsilon) * f_\zeta(\varepsilon). \tag{14}
$$

Here, $f_\epsilon(\varepsilon)$ can be approximated by $f_\chi(\varepsilon)$ because the variance of χ is much greater than that of ζ, and as a result, (13) reduces to

$$
\hat{\underline{z}}_{\mathrm{ML}} \approx \underset{\underline{z}}{\arg\min} \left[\sum_{i \in \Omega} \left[\ln(r_i - \parallel \underline{z} - \underline{p}_i \parallel) \right. \right.
$$
$$
+ \frac{1}{2\sigma_\chi^2} \left(\ln(r_i - \parallel \underline{z} - \underline{p}_i \parallel) - \mu_\chi \right)^2 \right]
$$
$$
\left. + \sum_{j \in \Omega} \frac{1}{2\sigma_\zeta^2} (r_j - \parallel \underline{z} - \underline{p}_j \parallel)^2 + \lambda \parallel \underline{z} - \underline{u}_1 \parallel \right]. \tag{15}
$$

Ⅵ. Results and discussion

Figs. 5 and 6 show the test results on the measurements taken at the lobby of the law school library and Hyoam chapel. In each case, two receivers were blocked by a person or object. The large ranging errors at the blocked beacons made the
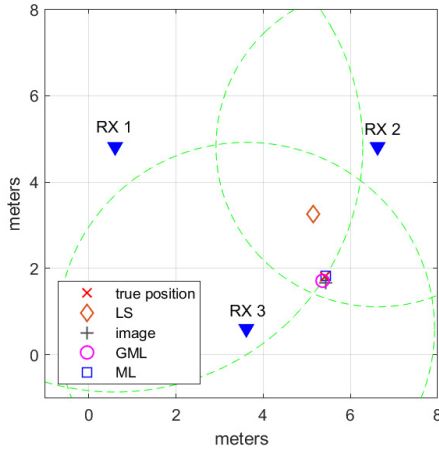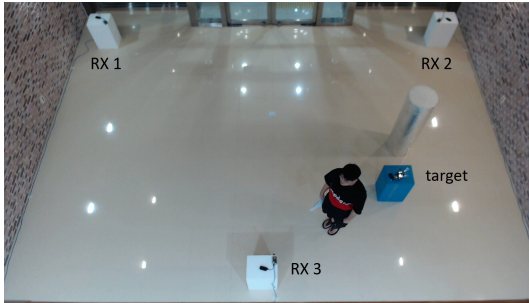
Fig. 5. The experimental setup of measurement at the lobby of law school library (upper) and the test result on the measured data (lower).
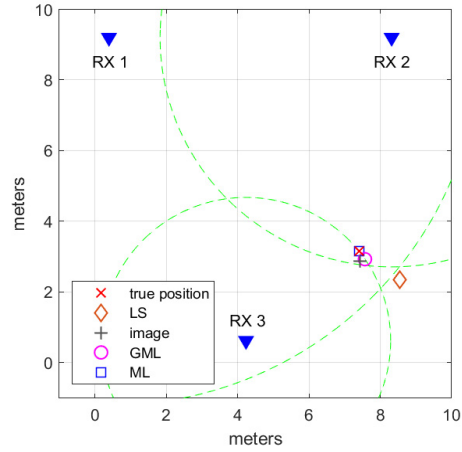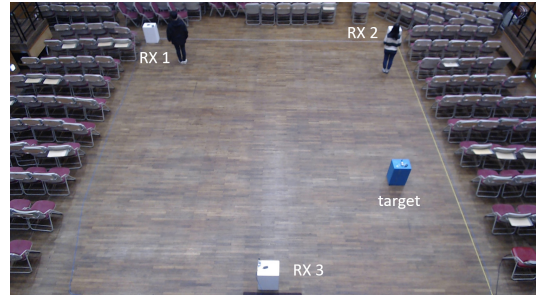

Fig. 6. The experimental setup of measurement at Hyoam chapel (upper) and the test result on the measured data (lower).

LS estimate very inaccurate; however, we can see that the GML and ML estimations combining both the image and UWB data have significantly improved the accuracy.

Fig. 7 compares the performance, measured by the root mean square (RMS) error, of the estimation methods. Seventy measurement samples were classified according to the number of blocked beacons, and the average RMS error was calculated. Applying the LS estimation to the UWB data in the absence of the LoS blockage, the RMS error was 0.0206 m; however, in the presence of the LoS blockage, the error was significantly increased. On the other hand, when only image data was used for the estimation, similar RMS error values were observed regardless of the number of blocked beacons, because distance measurements were used. Notice that the integration of UWB and image data

improved the accuracy compared to using only one of them; for example, with one blocked beacon, the RMS errors of the GML and ML methods were 0.0236 m and 0.0228 m, respectively, which are very close to the value obtained without obstacles.
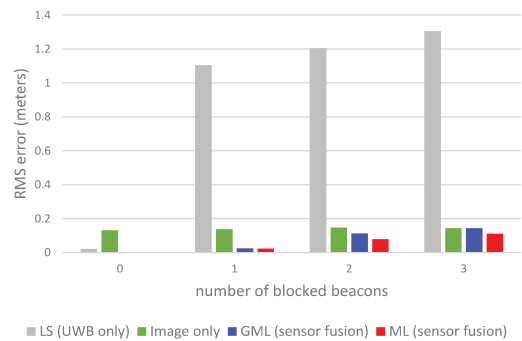

Fig. 7. Comparison of the RMS error performance of the positioning algorithms according to the number of blocked beacons.

Comparing the GML and ML methods, the ML method showed a fairly better performance than GML, but not significantly better. This appears to be due to the large variance of the non-LoS bias error.

The performance of the algorithm presentesd in this paper can be affected by a number of factors in addition to the number of blocked beacons: multipath structure of environment, the size and material of obstacle, distance between beacon and obstacle, and etc. It would be of interest to characterize the effects of these factors.

References

[1] J.-Y. Lee and R. A. Scholtz, "Ranging in a dense multipath environment using an UWB radio link," in *IEEE J. Sel. Areas in Commun.*, vol. 20, no. 9, pp. 1677-1683, Dec. 2002.

[2] J. Lee, Y. Jo, S. Kang, A. Kang, D. Ha, and S. Yoon, "Determination of the existence of LoS blockage and its application to UWB localization," *MILCOM 2006*, pp. 1-4, Washington DC, 2006.

[3] S. Maranò, W. M. Gifford, H. Wymeersch, and M. Z. Win, "NLOS identification and mitigation for localization based on UWB experimental data," in *IEEE J. Sel. Areas in Commun.*, vol. 28, no. 7, pp. 1026-1035, Sep. 2010.

[4] I. Guvenc, C. Chong, and F. Watanabe, "NLOS identification and mitigation for UWB localization systems," *2007 IEEE Wireless Commun. and Netw. Conf.*, pp. 1571-1576, Kowloon, 2007.

[5] Y.-H. Jo, J.-Y. Lee, D.-H. Ha, and S.-H. Kang, "Accuracy enhancement for UWB indoor positioning using ray tracing," *J. KICS*, vol. 31, no. 10C, pp. 921-926, 2006.

[6] L. Mucchi and P. Marcocci, "A new parameter for UWB indoor channel profile identification," in *IEEE Trans. Wireless Commun.*, vol. 8, no. 4, pp. 1597-1602, Apr. 2009.

[7] J. D. Hol, T. B. Schön, and F. Gustafsson, "Ultra-wideband calibration for indoor positioning," *2010 IEEE Int. Conf. Ultra-Wideband*, pp. 1-4, Nanjing, 2010.

[8] J. A. Corrales, F. A. Candelas, and F. Torres, "Hybrid tracking of human operators using IMU/UWB data fusion by a Kalman filter," *2008 3rd ACM/IEEE Int. Conf. Human-Robot Interaction* (HRI), pp. 193-200, Amsterdam, 2008.

[9] M. Kok, J. D. Hol, and T. B. Schön, "Indoor positioning using ultrawideband and inertial measurements," *IEEE Trans. Veh. Technol.*, vol. 64, no. 4, pp. 1293-1303, Apr. 2015.

[10] A. De Angelis, J. Nilsson, I. Skog, P. Händel, and P. Carbone, "Indoor positioning by ultrawide band radio aided inertial navigation," *Metrology and Measurement Syst.*, vol. 17, no. 3, pp. 447-460, 2010.

[11] C. Kim and J.-Y. Lee, "ToA-based multi-target localization and respiration detection using UWB radars," *EURASIP J. Wireless Commun. and Netw.*, vol. 2014, no. 145, pp. 1-15, 2014.

[12] I. E. Sutherland, "Three-dimensional data input by tablet," in *Proc. IEEE*, vol. 62, no. 4, pp. 453-461, Apr. 1974.

[13] N. A. Alsindi, B. Alavi, and K. Pahlavan, "Measurement and modeling of ultrawideband toa-based ranging in indoor multipath environments," in *IEEE Trans. Veh. Technol.*, vol. 58, no. 3, pp. 1046-1058, Mar. 2009.

김 대 웅 (Dae-Woong Kim)

2017년 2월 : 한동대학교 전산자공학부 (공학사)

2019년 8월 : 한동대학교 정보통신공학과 (공학석사)

2019년 8월~현재 : ㈜노드톡스 연구원

<관심분야> UWB 위치추적 시스템, 저전력 무선통신

[ORCID:0000-0002-3994-2594]

이 준 용 (Joon-Yong Lee)

1993년 2월 : 홍익대학교 전자공학과 학사 졸업

1997년 5월 : University of Southern California 전자공학과 석사 졸업

2002년 5월 : University of Southern California 전자공학과 박사 졸업

2002년 9월~현재 : 한동대학교 전산전자공학부 교수

<관심분야> 무선 위치추적시스템, UWB 레이더 센서네트워크

[ORCID:0000-0003-3469-8147]